ACS OMEGA

Open Access

http://pubs.acs.org/journal/acsodf

Article

Antitumor Effects of Tryptanthrin on Colorectal Cancer by Regulating the Mitogen-Activated Protein Kinase Signaling Pathway and Targeting Topo I and IDO1

Simeng Lu,[1] Bao-Long Hou,[1] Ting Wang,[1] Keyu Ma, Anli Huang, Xue Wu,* Yan-Ni Liang,* and Zheng Wang*

Cite This: *ACS Omega* 2025, 10, 3206−3221

Read Online

ACCESS | Metrics & More | Article Recommendations

ABSTRACT: Tryptanthrin (TRYP) is an indole quinazoline alkaloid with a range of pharmaceutical activities, but the specific mechanism of TRYP against colorectal cancer (CRC) remains obscure. The purpose of this study was to evaluate the antitumor effects of TRYP on CRC models both *in vitro* and *in vivo* and further analyze its concrete mechanisms. The results of the *in vitro* experiment show that TRYP effectively inhibited the proliferation and migration of SW620 cells, arrested the cell cycle at the S phase, and induced cell apoptosis. Deeply, TRYP dramatically increased the expression of Bax and cleaved caspase 3 while decreasing the expression of Bcl-2. The results of transcriptome sequencing implied that the inhibitory effects of TRYP were closely related to the mitogen-activated protein kinase (MAPK) signaling pathway, and the results of western blotting verified that TRYP could decrease the expression of p-Erk and increase the expression of p-p38 and p-Jnk. Besides, our results identified that topoisomerase I (Topo I) and indole amine 2,3-dioxygenase 1 (IDO1) were the targets of TRYP. *In vivo*, the results showed that different TRYP doses significantly inhibited tumor growth in mice, induced different degrees of necrosis in tumor tissues, decreased the expression level of Ki67 protein, and increased the apoptotic signal in tumor tissues. The findings demonstrated the inhibitory effects of TRYP on CRC, and the mechanisms were tightly connected to inhibiting the activity of Topo I and IDO1 and regulating the expression of the MAPK signaling pathway. Especially, it was first identified that TRYP could directly inhibit Topo I to arrest SW620 at the S phase. Therefore, this work established a scientific basis for the development of TRYP.

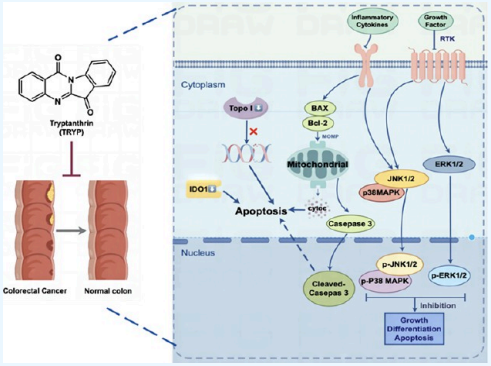

1. INTRODUCTION

Colorectal cancer (CRC) ranks as the third most widespread malignant disease globally, following lung cancer and breast cancer, and is associated with a significant mortality rate. Recent shifts in dietary patterns have led to an alarming rise in CRC incidence, particularly among younger individuals.[1] The etiology of this disease is multifaceted, often linked to dysregulated cellular proliferation and apoptosis, which involves complex proto-oncogenes, oncogenes, mismatch repair genes, and various modifying genes.[2] In recent years, individuals suffering from inflammatory bowel disease (IBD) have been identified as having an increasingly elevated risk of developing CRC.[3] Chronic inflammation is a critical factor in numerous stages of tumorigenesis, influencing cell differentiation, survival, proliferation, invasion, and angiogenesis.[4] Consequently, the effective management of IBD may mitigate the risk of subsequent colon cancer development. It is therefore imperative to identify safer and more efficacious therapeutic strategies to prevent both the onset and progression of CRC.[5]

Heterocyclic compounds are an important chemical class of drugs in medicinal chemistry and have magnificent applications in various sciences.[6−8] In the past decade, a number of nitrogen-containing heterocyclic small-molecule pharmaceuticals were approved by the U.S. Food and Drug Administration (FDA).[9,10] As a natural indole alkaloid containing nitrogen heterocycles, tryptanthrin (indolo [2,1-*b*]quinazoline-6,12-dione, TRYP) possesses the pharmacophores of quinazoline and indole[11,12] and exhibits a wide range of biological and pharmacological activities, such as antitumor, antibacterial, and anti-inflammatory effects.[13,14] This compound is derived from several plant sources, such as *Baphicacanthus cusia* (Nees)

Received: December 11, 2024
Accepted: December 20, 2024
Published: January 10, 2025

Bremek, *Polygonum tinctorium* W.T. Aiton, and *Isatis indigotica* Fortune and constitutes a principal component of traditional Chinese medicine preparations like indigo naturalis and folium isatidis.[15] Over the past few years, extensive research has been undertaken to elucidate the antitumor effects of TRYP,[16] which have demonstrated its capacity to inhibit the production of nitric oxide and prostaglandin E2, thereby exhibiting anti-inflammatory properties.[17] In our previous study, it was found that TRYP could greatly improve the health conditions of colitis mice induced by dextran sodium sulfate. Also, the molecular mechanism of TRYP on colitis might be related to regulating IL-6/STAT3 and TNF-α/NF-κB signaling pathways.[18] Given the pivotal role of inflammation in cancer progression, TRYP was employed in this study to evaluate its therapeutic potential against the CRC.

Conserved signaling modules known as mitogen-activated protein kinase (MAPK) link extracellular stimuli to the regulatory apparatus, controlling vital cellular processes such as migration, apoptosis, cell cycle arrest, and proliferation.[19,20] The most well-characterized MAPK subfamilies in mammals include extracellular signal-regulated kinase (Erk), c-Jun N-terminal kinases (Jnk), and P38 MAPK.[21] Also, all of them have been involved in cancer, in particular, in colorectal cancer, the function of Erk inhibiting tumor growth *in vitro*, the function of Jnk inducing tumor cell apoptosis, and the function of P38 MAPK blocking the cell cycle and inhibiting tumorigenesis.[22] Notably, TRYP has been shown to modulate MAPK protein levels in models of imiquimod-induced inflammation.[23] However, the cytotoxic effects of TRYP on colon cancer cells and the specific mechanisms underlying these effects remain inadequately defined.

Topoisomerase I (Topo I) is crucial for maintaining DNA topology, as it transiently cleaves one strand of DNA, allowing relaxation of the supercoiled DNA before resealing it.[24] Beyond these normal functions, Topo I serves as a significant cellular target in the treatment of human cancers.[25] Its inhibition can lead to DNA strand breaks, thereby disrupting tumor cell division and ultimately inducing tumor cell apoptosis.[26] In the present study, we observed that TRYP effectively arrested SW620 cells at the S phase.[27] Furthermore, 10-hydroxycamptothecin (10-HCPT) is a widely utilized Topo I inhibitor drug.[28] Based on the similarity in the chemical structures of TRYP and 10-HCPT, it was predicted that the antitumor effects of TRYP might be correlated to Topo I inhibition.

Indole amine 2,3-dioxygenase 1 (IDO1) is a crucial enzyme in the metabolism of tryptophan.[29] It catalyzed the initial and rate-limiting step of the kynuridine pathway of tryptophan metabolism by oxidizing tryptophan to *N*-formylkynuridine.[30] As a key regulator of immune responses, IDO1 is an important therapeutic target for inflammation and cancer.[31] It was similarly reported to be inhibited by TRYP and its derivatives.[32,33]

Therefore, building on prior findings and the existing literature, this study aims to evaluate the impacts of TRYP on CRC both *in vitro* and *in vivo*. The underlying molecular mechanisms include regulation of MAPK, Topo I, and IDO1 activities. These results could provide evidence supporting the development and use of TRYP as a potential drug for treating CRC.

2. MATERIALS AND METHODS

2.1. Materials. TRYP was synthesized by the Pharmaceutical Chemistry Laboratory of the Shaanxi Collaborative Innovation Centre of Medicine Resources Industrialization (Xianyang, Shaanxi, China). RPMI 1640 medium, trypsin-EDTA, and fetal bovine serum (FBS) were purchased from Biological Industries (Kibbutz Beit Haemek, Israel). MTT reagent was purchased from Beijing Suolaibao Technology Company (Beijing, China). Dimethyl sulfoxide (DMSO) was purchased from Annoron Biotechnology (Beijing, China). Cell cycle kits were purchased from Beyotime Biotechnology (Shanghai, China). The Apoptosis Assay Kit was purchased from Novozymes Biotechnology (Nanjing, Jiangsu, China). RIPA lysis buffer, phosphatase inhibitor, proteinase inhibitor, BCA protein quantitative kit, ECL chemiluminescence kit, and β-actin antibody were purchased from BOSTER Biological Technology Company (Wuhan, Hubei, China). The SDS-PAGE Gel Preparation Kit was purchased from Mishushengwu Company (Xian, Shaanxi, China). The antibodies of Bcl-2, Bax, P38, Topo I, and IDO1 were purchased from Abcam (Cambridge, MA, United States). The antibodies of caspase 3 and cleaved caspase 3 were purchased from Cell Signaling Technology (Danvers, MA, United States). The antibodies of p-P38, p-Jnk, and p-Erk were purchased from Wanlei Biotechnology (Shenyang, Liaoning, China). The antibodies of Jnk and Erk were purchased from the Proteintech Group Inc. (Wuhan, Hubei, China). pBR322 DNA was purchased from Takara Biotechnology (Beijing, China). 10-HCPT, ascorbic acid, methylene blue, catalase, L-tryptophan, and *p*-dimethylaminobenzaldehyde were purchased from Yuan Ye Biotechnology (Shanghai, China). IDO1 was purchased from Sino Biological (Beijing, China).

2.2. Cell Culture and Animals. Human colorectal cancer cells SW620 were purchased from Guangzhou Gineo Biotechnology Company (Guangzhou, Guangdong, China). RPMI 1640 medium was utilized to propagate SW620 cells with injections of 10% FBS, 100 U/mL penicillin, and 100 μg/mL streptomycin. The cells were cultivated in a humidified atmosphere containing 5% CO_2 at 37 °C. Male nude mice (BALB/c, 16 + 2 g) aged 4−6 weeks (no. SCXK-2020-030) were provided by Chengdu Dashuo Laboratory Animal Company (Chengdu, Sichuan, China), and all procedures involving animals were carried out in compliance with guidelines authorized by the animal ethics committee of Shaanxi University of Chinese Medicine (no. SUCMDL20221201001). The animals were kept in sterile settings with a temperature of (24 ± 2) °C, humidity of (50 ± 10) %, and a 12 h light/dark cycle. They also had unrestricted access to water and normal rodent chow.

2.3. Cell Viability Assay. SW620 cells were transferred in a 96-well microplate with 1.5 × 10^5 cells/well, allowed to attach overnight, and then treated with diverse concentrations of TRYP for 24, 48, and 72 h. Following treatment, each well received 15 μL of MTT, and the wells were incubated at 37 °C for 4 h. Following the elimination of the agent, 150 μL of DMSO was applied. After the 10 min incubation period with moderate agitation, the absorbance at 490 nm was measured from a microplate reader (Thermo Fisher Scientific, Waltham, MA, United States). The following formula was used to figure out the inhibition rate:

$$\text{inhibitionrate}\ (\%) = (A_{\text{CON}} - A_{\text{Treated}})/A_{\text{CON}} \times 100\%$$

https://doi.org/10.1021/acsomega.4c11189
ACS Omega 2025, 10, 3206−3221

2.4. Wound Healing Assays. After SW620 cells were transplanted into six-well plates, the cells were grown there all night. The tip of a 10 μL pipet was utilized to scratch the monolayer of SW620 cells, and phosphate-buffered saline (PBS) was subsequently utilized to rinse the floating cells. Under a microscope, the gap widths were measured. During treatment using multiple concentrations of TRYP (0, 5.36, 10.72, and 16.09 μM), the gap widths of cells were evaluated at 0, 24, and 48 h.

2.5. Cell Cycle Assays. SW620 cells were cultivated in a 6-well plate with 1×10^6 cells/well and were incubated with various doses of TRYP (0, 5.36, 10.72, and 16.09 μM) for 48 h. Next, the cells were subsequently placed back in 75% ethanol (4 °C) for stabilization after being washed twice with PBS. After a 5 min centrifugation at 1000 rpm at 4 °C, the cells were collected and flushed with PBS. Subsequently, the cells received therapy for 30 min at 37 °C in a cell incubator with propidium iodide staining solution. The evaluation of the samples was performed with a BD FACSVerse flow cytometer.

2.6. Measurement of Apoptosis. SW620 cells were seeded in a 6-well plate with 1×10^6 cells/well and were incubated with various concentrations of TRYP (0, 5.36, 10.72, and 16.09 μM) for 48 h. Centrifuging the SW620 cells for 10 min at 4 °C at 1000 rpm was the method utilized to harvest them. After this, a component of the cells was again suspended in PBS and centrifuged repeatedly. Subsequently, the suspended cells were then combined with 1× Binding Buffer and Annexin V-FITC, respectively. After 15 min in the dark, the suspended cells were treated with propidium iodide for staining. For the procedures, a BD FACSVerse flow cytometer was implemented.

2.7. Western Blot Analysis. After being lysed in RIPA solution incorporating protease and phosphatase inhibitors, the treated cells were separated through electrophoresis on sodium dodecyl sulfate−polyacrylamide gel electrophoresis (SDS-PAGE) gels and transferred onto poly(vinylidene difluoride) (PVDF) membranes. The cells were immobilized with 5% milk for 2 h at a 37 °C thermostat and flushed three times with 1× Tris-buffered saline with Tween 20. The primary antibody solution (1:1000) was incubated on the PVDF membranes for a whole night at 4 °C. The secondary antibody solution (1:1000) was subsequently applied for 1 h at 37 °C. The Bio-Rad Gel Imaging System was utilized to analyze protein expression.

2.8. Transcriptome Analysis. The SW620 cells were seeded in six-well plates to divide into a control group and a drug-treatment group. The drug-treated groups added 16.09 μM TRYP for 24 h. The cells were collected and centrifuged, and 1 mL of TRIzol was added to allow the cells to be fully lysed in TRIzol. It was sent to Ovison Biologicals for transcriptome sequencing to screen for differential genes and analyze the molecular mechanisms.

2.9. DNA Topo I Activity Assay. The total volume of the reaction mixture contained 2 μL of 10× DNA Topo I buffer, 2 μL of 0.1% bovine serum albumin, 0.5 μL of pBR322 DNA, 1 μL of Topo I (0.5 U), and 1 μL of TRYP (0.45, 0.9, and 1.8 mM), and then distilled water was added to a total volume of 20 μL. The reaction mixtures were placed in a 37 °C thermostat for 30 min. Ten microliters of the mixture was absorbed into a 1% agarose gel sample tank and electrophoresed at 100 V for 50 min.[34] After GelRed staining for 30 min, the electrophoretic gel images were observed and photographed under ultraviolet light.

2.10. IDO1 Activity Assay. The total volume of the reaction mixture contained 20 μL of potassium phosphate buffer (500 mM), 20 μL of ascorbic acid (200 mM), 4 μL of methylene blue solution (0.5 mM), 4 μL of catalase, 112 μL of H_2O, 20 μL of IDO1, 10 μL of TRYP (0, 2, 4, 8, 16, 32, 64, and 128 μM), and 10 μL of L-tryptophan (4 mM). The reaction mixtures were placed in a 37 °C thermostat for 1 h. Next, the supernatant was taken, mixed with 30% trichloroacetic acid, reacted at 60 °C for 30 min, and mixed with a 2% *p*-dimethylaminobenzaldehyde acetic acid solution.[35] After a 5 min incubation period with moderate agitation, the absorbance at 480 nm was detected with a microplate reader (Thermo Fisher Scientific, Waltham, MA, United States). The inhibition rate was calculated using the following formula:

$$\text{inhibitionrate}\ (\%) = (A_{\text{CON}} - A_{\text{Treated}})/A_{\text{CON}} \times 100\%$$

2.11. Molecular Docking Analysis and ADMET. Topo I (Protein Data Bank (PDB): 1K4T) and IDO1 (PDB: 4U74) structures were obtained from the PDB database. The small-molecule TRYP structure was generated in three dimensions using the open-source cheminformatics software package RDKit and conformationally sampled. Molecular docking experiments were performed using AutoDock version 4.2 software. The best binding site was predicted by using SiteMap software. Conformational sampling and scoring were performed by using genetic algorithms. Additionally, conformational sorting by applying docking scores was implemented to identify the most advantageous conformations. *In silico* ADME was investigated using SwissADME (http://www.swissadme.ch).

2.12. Molecular Dynamics (MD) Simulation. Molecular dynamics (MD) simulations were performed by using Gromacs2021. Proteins and DNA use AMBER force fields, and small molecules use GAFF force fields. The small protein molecule complex formed by docking molecules was placed in a suitable-sized molecular dynamics simulation box. Each system was solvated with TIP3P water in the simulation box under periodic boundary conditions, followed by the use of sodium chloride to neutralize the charge of the simulation system. After the simulation system was constructed, the steepest descent algorithm was used to minimize the energy of the two simulation systems. After energy minimization, the NVT and NPT systems and standard coupling methods (temperature: 300 K; pressure: 1 atm) were used to balance the molecules in the two simulated systems at 100 ps each. Finally, the tracks were generated with a time step of 2 fs, the number of frames was saved every 10 ps, and the molecular dynamics simulation was performed at 50 ns.[36]

2.13. Animal Experimental Studies. The animal model was established by inoculating SW620 (1×10^6 cells/mL) into the right armpit of each mouse. After 2 weeks, the size of the tumor approaching 30−40 mm^3 revealed that the model was successful. Then, the mice were randomly divided into 5 groups (10 mice of each group). The TRYP-treated mice were intraperitoneally injected with different dosages of TRYP (50, 100, and 200 mg/kg body weight). The positive control group was treated with 6 mg/kg 10-HCPT, and the model control group was administered a 0.9% saline solution. Then all mice were euthanized for sample collection at the end of day 18. The liver, kidney, and spleen were removed immediately and weighed. The weight of the spleen and thymus in connection with body weight was used to figure out the kidney, liver, and

https://doi.org/10.1021/acsomega.4c11189
ACS Omega 2025, 10, 3206−3221

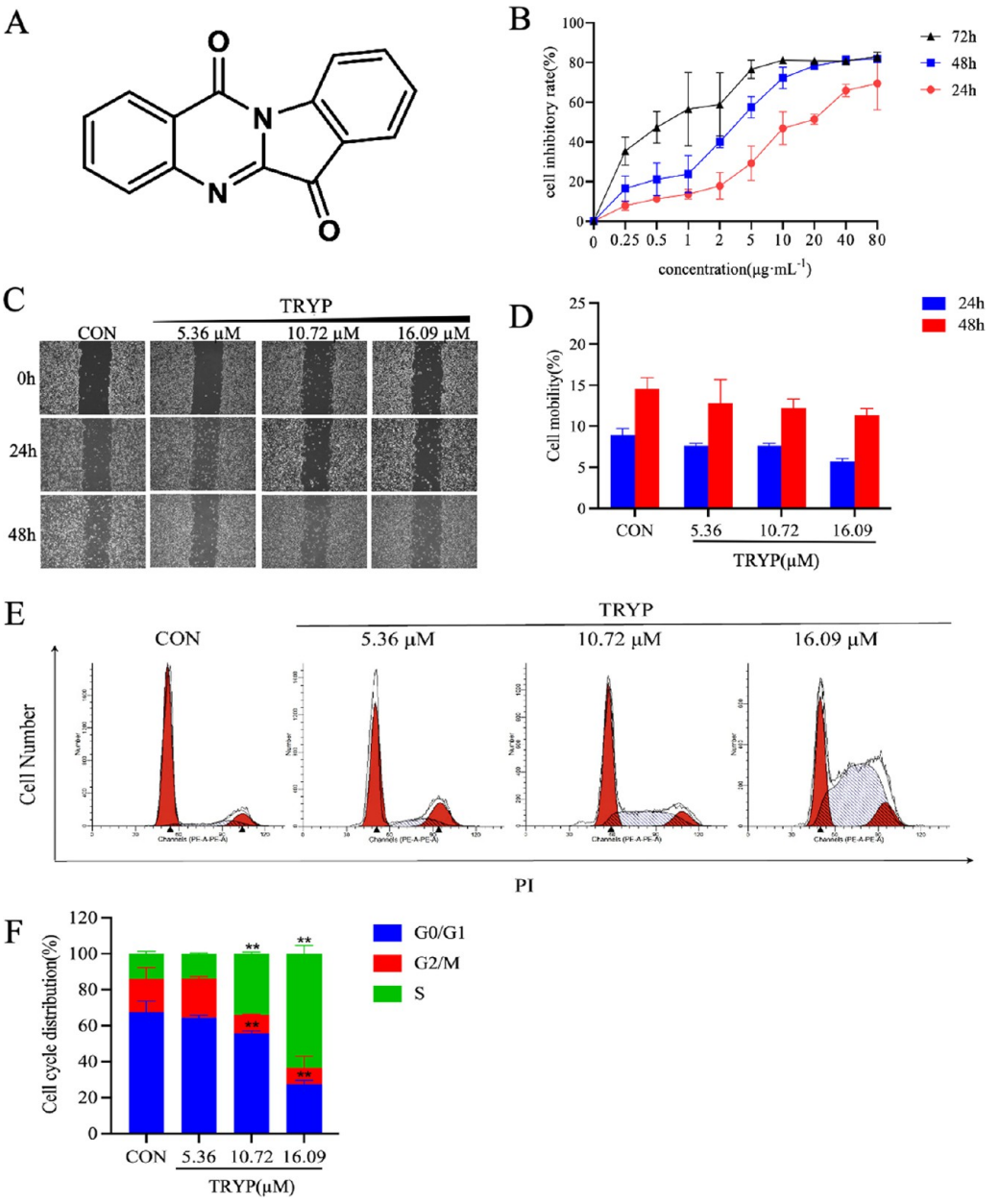

Figure 1. TRYP regulated proliferation, migration, and cell cycle progression of SW620 cells. (A) Chemical structures of TRYP. (B) Cell viability assay showed that TRYP had an inhibitory effect on the proliferation of SW620 cells. (C, D) Wound healing assays were used to verify the effects on migration of SW620 cells. (E, F) Flow cytometry was used to examine the effects of TRYP on SW620 cell cycle progression. All data were presented as the means ± SD (n = 3; *P < 0.05 and **P < 0.01).

spleen indexes. To ascertain the inhibitory effect of TRYP on tumors, the inhibition rate was expressed as follows:

$$\text{tumor inhibitory rate (\%)} = (W_{\text{CON}} - W_{\text{Treated}})/W_{\text{CON}} \times 100\%$$

2.14. Hematoxylin and Eosin (H&E) Staining. Samples from tumor tissue were embedded in paraffin, sectioned, fixed in a 4% polyformaldehyde solution, and stained with hematoxylin and eosin (H&E) for histopathological examination. The sections were observed under a microscope to differentiate the morphological structure of normal tissue and pathological colon tissue. The following parameters were utilized to evaluate histological damage: crypt destruction, inflammation intensity, and inflammation extent.

2.15. Immunohistochemistry (IHC) Analysis. Paraffin sections of tumor tissue from mice were cleaned with PBS, soaked in a 3% hydrogen peroxide solution, and then incubated overnight at 4 °C with the essential antibody and the subsequent day with the secondary antibody. The sections were stained with 3,3′-diaminobenzidine and then retained with hematoxylin. Images were acquired under a microscope, and the area ratio of positive areas of Ki67 was analyzed in each group of images using Image-Pro Plus version 6.0.

2.16. Terminal Deoxynucleotidyl Transferase-Mediated dUTP Nick-End Labeling (TUNEL) Assay. Paraffin sections of tumor tissue from mice were dried with water. The fixed tissue area was dripped with protease K and incubated at 37 °C for 25 min. Then, the film breaking solution was incorporated. The sections were completely infiltrated with

https://doi.org/10.1021/acsomega.4c11189
ACS Omega 2025, 10, 3206−3221

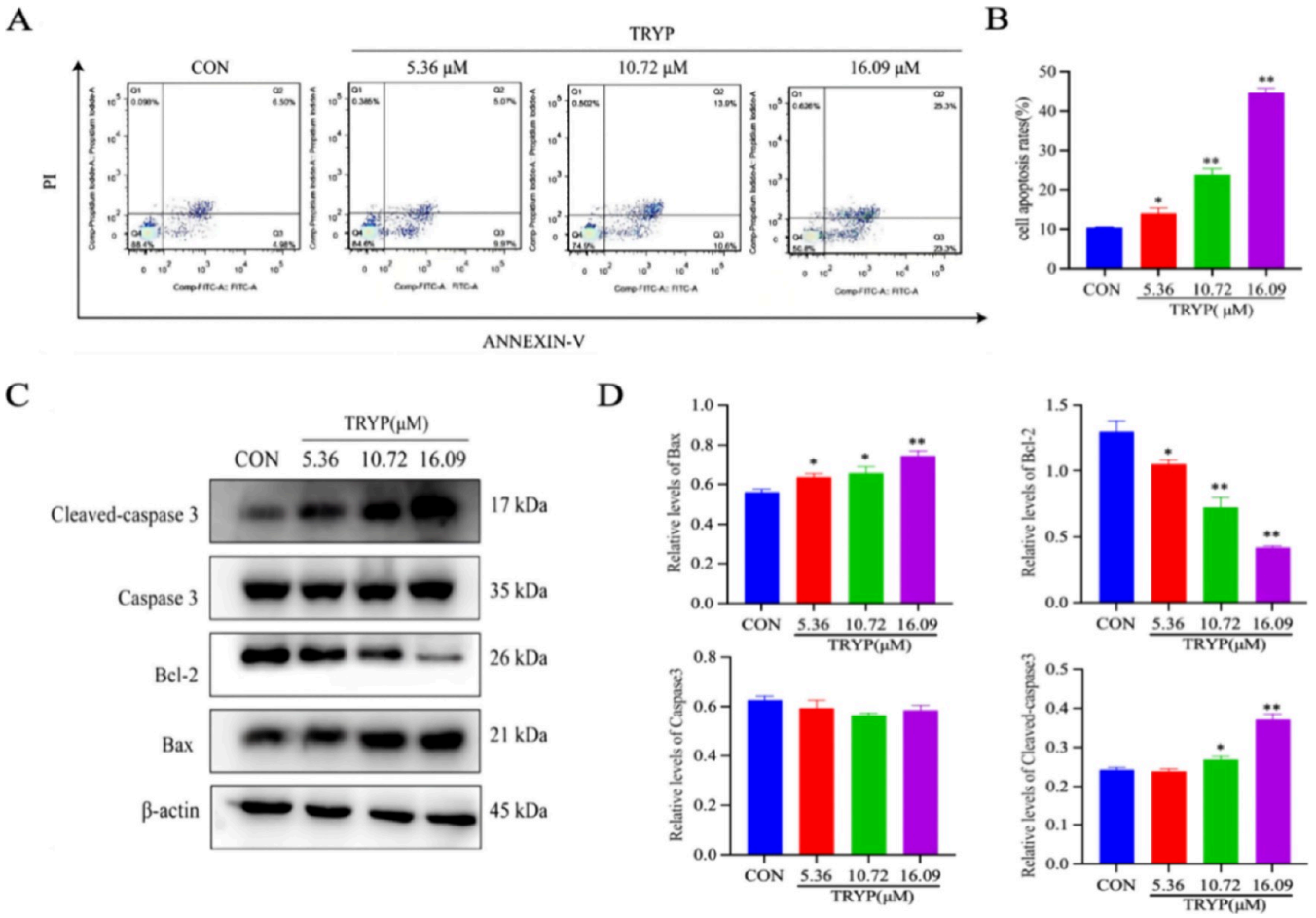

Figure 2. TRYP induced the apoptosis of SW620 cells. (A, B) Flow cytometry was used to detect the effect of TRYP on the apoptosis of SW620. All data were presented as the means ± SD (n = 3; *P < 0.05 and **P < 0.01). (C, D) Expression levels of proteins associated with the apoptotic mitochondrial pathway. All data were presented as the means ± SD (n = 3; *P < 0.05 and **P < 0.01).

mixed TdT reagent 1 and dUTP reagent 2. 4′,6-Diamidino-2-phenylindole stain was added dropwise and incubated for 10 min away from light. The positive area ratio of terminal deoxynucleotidyl transferase-mediated dUTP nick-end labeling (TUNEL) in each group of images was analyzed with Image-Pro Plus 6.0.

2.17. Statistical Analysis. All data were presented as the means ± standard deviation (SD) of three individual experiments. The statistical differences were analyzed by one-way ANOVA using GraphPad Prism 8.0 (San Diego, CA, United States). *P < 0.05 was regarded as different, and **P < 0.01 was considered as significantly different.

3. RESULTS

3.1. TRYP Regulated Proliferation, Migration, and Cell Cycle Progression on SW620 Cells. To verify the potential anticancer activity of TRYP (Figure 1A), the effects of TRYP on the proliferation and migration of SW620 cells were determined. As shown in Figure 1B, TRYP had an inhibitory effect on the proliferation of SW620 cells in a time- and concentration-dependent manner. Also, the inhibitory concentration (IC_{50}) values were 53.06, 16.09, and 3.67 μM, following 24, 48, and 72 h of TRYP treatment, respectively. We finally conducted follow-up experiments on IC_{50} at 48 h, and 5.36, 10.72, and 16.09 μM were selected as the final TRYP concentrations. As shown in Figure 1C,D, the mobility rates of 24 h groups were 8.90, 7.61, 7.60, and 5.73%. Also, those of 48 h groups were 14.60, 12.85, 12.22, and 11.30% after treatment with different concentrations of TRYP (5.36, 10.72, and 16.09 μM). The result indicated that SW620 cells had characteristics of aggregation growth and were difficult to migrate.

The detrimental impacts of TRYP on the cell cycle were established using flow cytometry. As shown in Figure 1E,F, the proportion of cells blocked at the S phase was significantly increased to (33.82 ± 0.94 and 63.57 ± 4.61%) compared with that in control (14.16 ± 1.18%). On the contrary, the percentage of cells at the G0/G1 phase was sharply decreased (55.90 ± 1.22 and 27.59 ± 2.08%), while that in the control group increased (67.52 ± 6.10%). The research findings pointed out that TRYP could arrest the cell cycle at the S phase in a dose-dependent manner.

3.2. TRYP Induced the Apoptosis of SW620 Cells. Apoptosis, a type of organized cell death governed through miscellaneous genes, constitutes a common mechanism associated with numerous anticancer medications.[37] Therefore, the effects of different doses of TRYP (5.36, 10.72, and 16.09 μM) on the apoptosis of SW620 cells were detected using flow cytometry. As shown in Figure 2A,B, the number of apoptotic cells was significantly higher in the TRYP group than that in the control group, and the apoptosis rates in all groups were 10.76, 14.08, 22.79, and 45.63%, respectively. As shown in Figure 2C,D, the western blot revealed that TRYP significantly

https://doi.org/10.1021/acsomega.4c11189
ACS Omega 2025, 10, 3206−3221

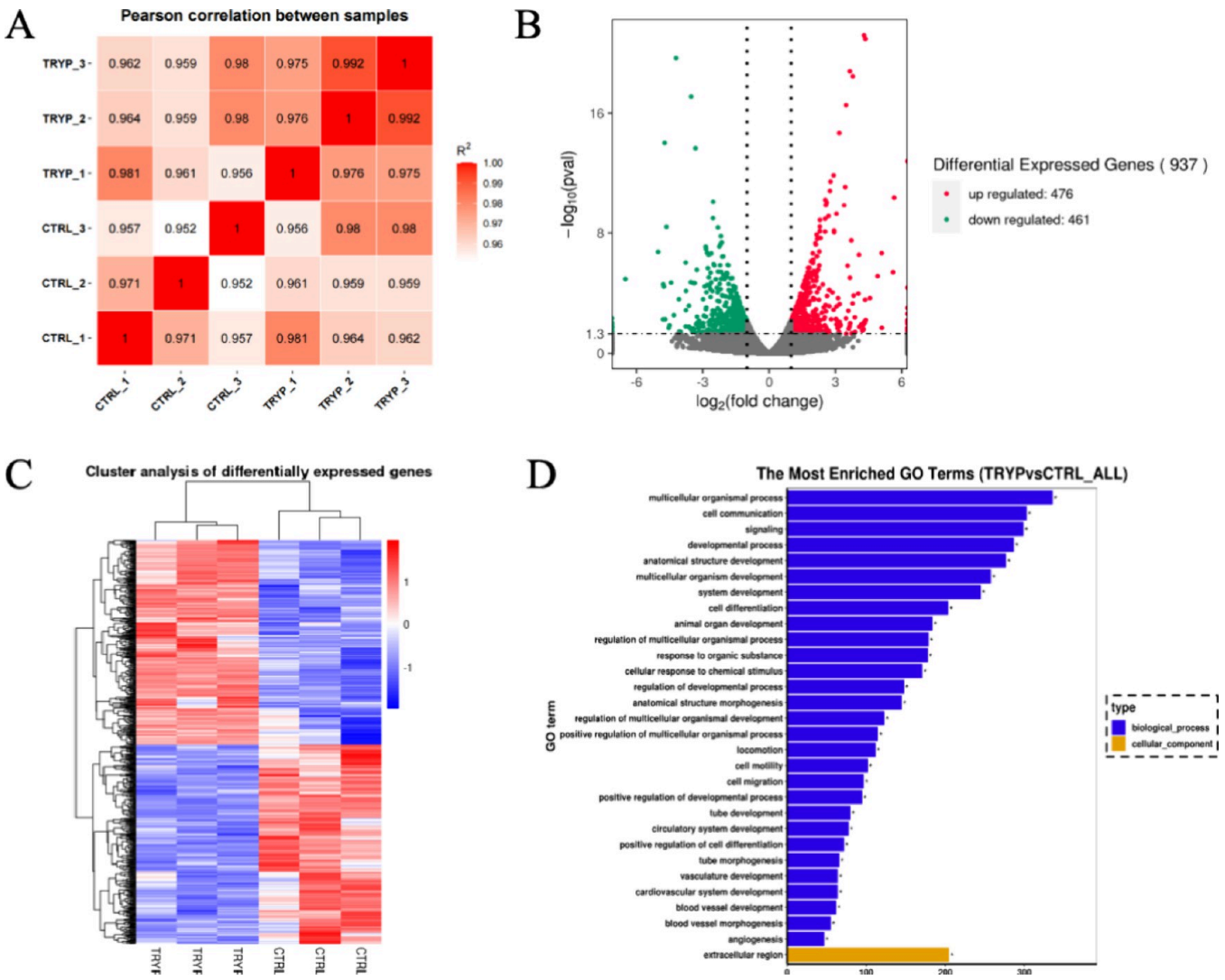

Figure 3. Transcriptome analysis reveals possible pathways involved in TRYP. (A) Biological repetition analysis chart. (B) Differential gene volcano map. (C) Differential gene heatmap. (D) GO enrichment analysis plot.

alleviated Bcl-2 expression levels while enhancing the expression of Bax and cleaved caspase 3 expression levels on SW620 cells, which were critical markers associated with apoptosis.

3.3. Transcriptome Analysis Reveals Possible Pathways Involved in TRYP. To further identify the mechanism of the inhibitory activity of TRYP on SW620 cells, differentially expressed genes after TRYP treatment were screened using transcriptome analysis. As shown in Figure 3A, the results indicated that the samples were highly correlated and reproducible, and the experimental results were reliable. The heatmap was applied to infer the general geographic distribution of differential genes (Figure 3C). As shown in Figure 3B, there were 937 differentially expressed genes affected by TRYP in SW620 cells, including 476 upregulated and 461 downregulated. The quantity and distribution of differential gene expression enriched in biological processes, cell components, and molecular functions may be intuitively reflected by a Gene Ontology (GO) analysis of DEGs. The results in Figure 3D suggested that the first 30 GO terms were mainly involved in biological processes, including cell proliferation, apoptosis, differentiation, migration, and adhesion.

3.4. TRYP Activated the MAPK Signaling Pathway to Exert Antitumor Effects on SW620 Cells. According to the transcriptome database analysis, the four most significantly altered genes were selected to determine the mechanism of TRYP on SW620 cells. The expression of HRK and CLDN7 sharply increased after TRYP treatment, whereas the expression of CYP24A1 and FOS significantly decreased in the TRYP group compared with that in the control group (Table 1). HRK was a downstream molecule of the Jnk signaling pathway, and its expression was increased after activation by Jnk, which induced apoptosis by releasing Bak in complex with Bcl-xl.[38,39] CLDN7 could act as an inhibitor of upstream elements of the Erk/MAPK pathway, thereby

Table 1. MAPK Signaling Pathway-Related Differential Genes

name	log2(fold change)	*P*-value	regulation
HRK	3.6596	0.00000947	UP
CLDN7	2.3264	0.000000021	UP
CYP24A1	−2.69	0.00002970	DOWN
FOS	−2.1895	0.00005310	DOWN

https://doi.org/10.1021/acsomega.4c11189
ACS Omega 2025, 10, 3206−3221

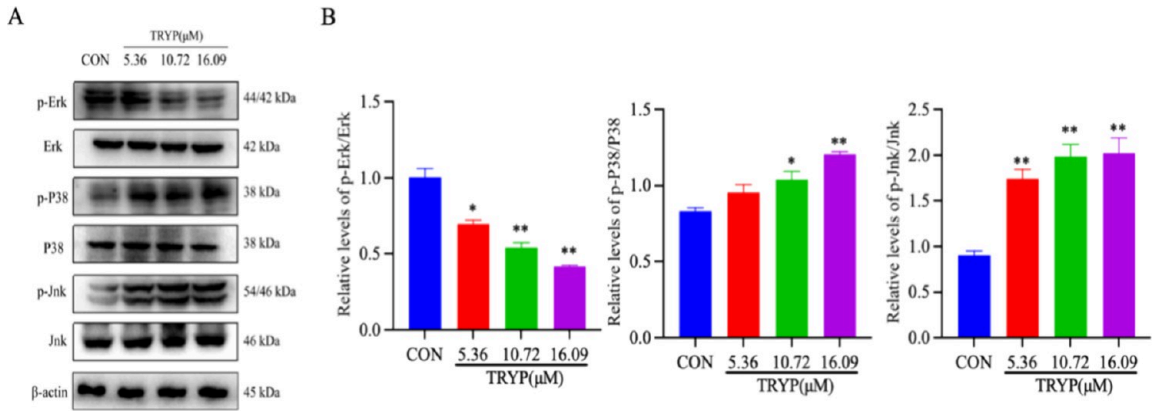

Figure 4. TRYP regulated the expression of proteins associated with the MAPK pathway. (A, B) TRYP regulated the expression levels of the MAPK pathway-related proteins. All data were presented as the means ± SD (n = 3; *P < 0.05 and **P < 0.01).

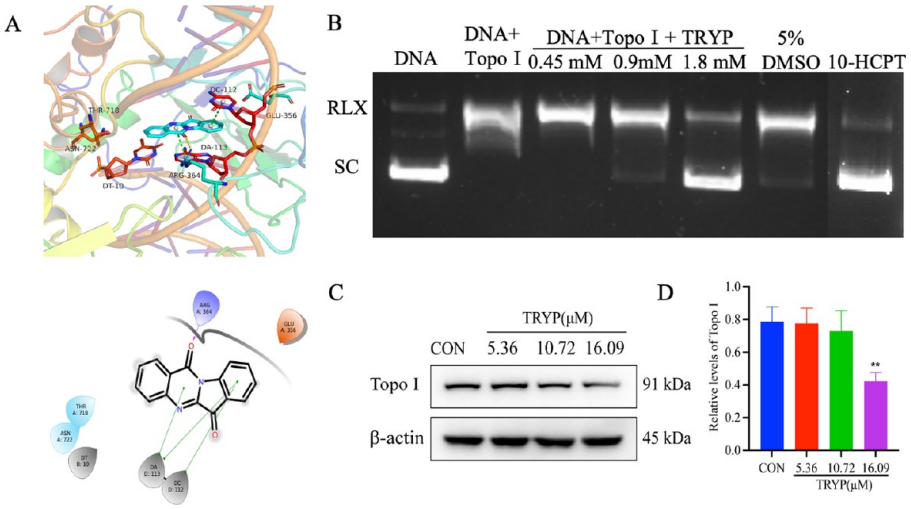

Figure 5. TRYP inhibited the activity of DNA Topo I to arrest the cell cycle at the S phase. (A) Binding interaction between TRYP and Topo I (PDB: 1K4T). (B) Effect of TRYP on the activity of Topo I. (C, D) Expression of Topo I protein. All data were presented as the means ± SD (n = 3; *P < 0.05 and **P < 0.01).

downregulating ERK activity and inhibiting cancer cell invasion and migration. CYP24A1 could inhibit the MAPK signaling pathway, downregulated Erk phosphorylation, and inhibited colon cancer cell proliferation.[40] FOS was a downstream signal regulator of Erk and played an important role in tumor formation and inhibition.[41,42] All of the selected genes were tightly connected to the MAPK signaling pathway.

Therefore, we determined which proteins are essential components in the MAPK signaling pathway. As shown in Figure 4A,B, TRYP decreased the expression levels of p-Erk and increased the levels of expression of p-P38 and p-Jnk. Inhibiting p-Erk could prevent tumor growth *in vivo*, while increasing p-Jnk and p-P38 could induce cell apoptosis and block the cell cycle. These results implied that the inhibitory effects of TRYP on SW620 cells were closely related to regulation of the MAPK signaling pathway.

3.5. TRYP Inhibited the Activity of DNA Topo I to Arrest the Cell Cycle at the S Phase. The results of cell cycle experiments have shown that TRYP could arrest SW620 cells at the S phase, and previous studies had shown that the activity of Topo I at the S phase was significantly increased.[43] Therefore, we hypothesized that the inhibitory effects of TRYP might be related to Topo I activation.

Computer-aided drug design is a key component of modern preclinical drug discovery, and different software applications and computational methods are usually combined to try to screen promising drug candidates.[44,45] In recent years, it has become an indispensable constituent in medicinal chemistry.[46,47] We analyzed the affinity of TRYP for Topo I (PDB: 1K4T) using molecular docking techniques. The binding interaction between TRYP and Topo1 is shown in Figure 5A. The carbonyl group of TRYP formed a hydrogen bond with the Arg364 side chain of the protein, while the charge centers of pyridine and benzene rings formed $\pi-\pi$ pairs with the charge centers of adenine and cytosine side chains of the DNA helix. As shown in Figure 5B, Topo I activity was inhibited after the treatment of TRYP. TRYP (1.8 mM) completely inhibited the unwinding of DNA pBR322 by Topo I, which was equivalent to the effect of 10-HCPT in the positive group. To further verify these inhibitory effects, the protein expression level of Topo I on SW620 cells was detected after TRYP treatment. As shown in Figure 5C,D, with the increased TRYP concentrations, the protein expression level of Topo I gradually decreased, and Topo I expression was significantly reduced by 16.09 μM TRYP. Based on the above results, it was concluded that TRYP could effectively inhibit Topo I, resulting in the cell

https://doi.org/10.1021/acsomega.4c11189
ACS Omega 2025, 10, 3206−3221

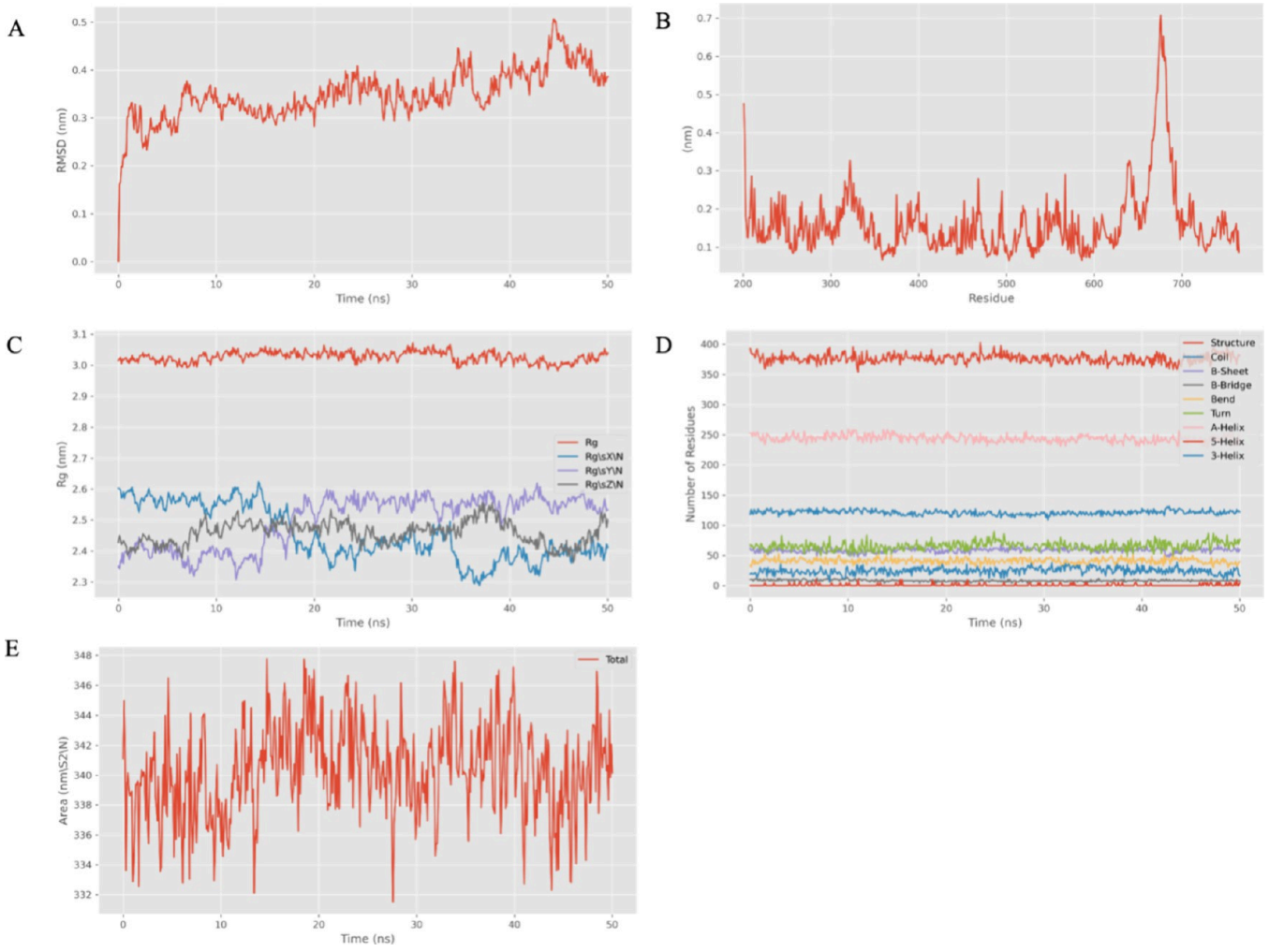

Figure 6. Molecular dynamics of DNA Topo I. (A) RMSD curve of small protein molecules over time. (B) RMSF curves of different protein residues. (C) R_g curve of proteins over time. (D) Number of secondary structures in a protein changes over time. (E) Variation of the solvent-accessible surface area of the protein over time.

cycle being blocked at the S phase and the proliferation of SW620 cells being inhibited.

Next, we simulated the molecular dynamical system of TRYP to Topo I. As shown in Figure 6A, the simulated root-mean-square deviation (RMSD) value was 0.39. After 10 ns, the change in RMSD value of the whole simulation system was basically less than 2 Å, indicating that the whole simulation system was relatively stable. It can be seen from Figure 6B that the root-mean-square fluctuation (RMSF) of residue 676 was relatively large, which indicated that there was random curling around this position. As shown in Figure 6C, the R_g value at the end of the simulation was 3.03974, and the fluctuation of R_g during the whole simulation was very small. Figure 6D shows how the number of secondary structures of protein changed over time. Figure 6E shows the variation of protein's solvent-accessible surface area over time, and the result displayed that the solvent-accessible surface area of proteins fluctuated little.

3.6. The Effects of TRYP Inhibited the Activity of IDO1 Closely Related to the MAPK Signaling Pathway. IDO1 was considered as a classical target of TRYP and its derivatives.[48] Previous studies had demonstrated that the inhibition of IDO1 could downregulate the expression levels of p-Erk on CRC cells.[49] Here, we evaluated the inhibitory effect of TRYP on IDO1 on SW620 cells.

Molecular docking was used to determine the combination of TRYP and IDO1 (PDB: 4U74). As shown in Figure 7A, a metal ion−π interaction was formed between the charge center of the benzene ring of TRYP and the central iron atom of the enzyme's cofactor HEME. Also, the charge center of the diazo hexamembered ring also formed a metal ion−π interaction with the iron ions in the center of the cofactor. In addition to $\pi-\pi$ stacking interaction with the charge center of the hydrophobic amino acid Phe163, the molecule formed hydrophobic contact interactions with other surrounding hydrophobic amino acids such as Leu234, Ala262, Ala264, Val130, and Phe164. As shown in Figure 7B, after different concentrations (0, 2, 4, 8, 16, 32, 64, and 128 μM) of TRYP were added into the reaction, the production of kynurenine was decreased in a dose-dependent manner, and the IC_{50} value of TRYP on IDO1 was 17.26 μM according to the inhibition rates. As shown in Figure 7C,D, the protein expression level of IDO1 on SW620 cells gradually decreased after 48 h of treatment with different concentrations of TRYP (5.36, 10.72, and 16.09 μM). The result demonstrated that TRYP could inhibit IDO1 on SW620 cells.

https://doi.org/10.1021/acsomega.4c11189
ACS Omega 2025, 10, 3206−3221

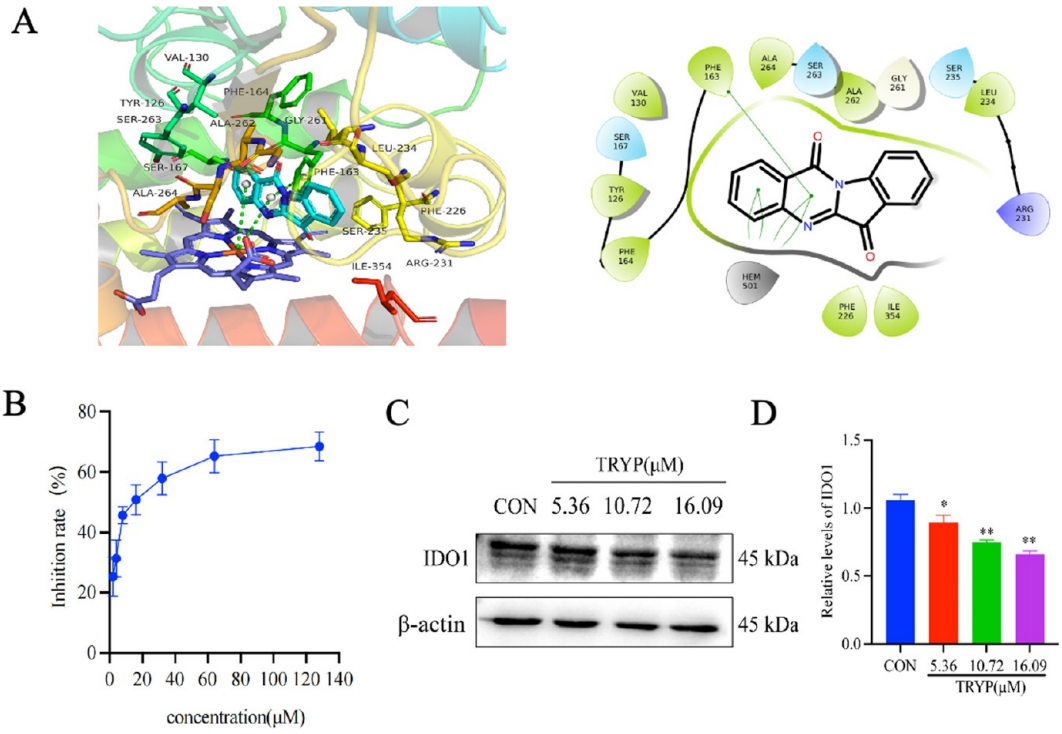

Figure 7. Effects of TRYP inhibiting IDO1 closely related to the MAPK signaling pathway. (A) Interaction of TRYP with IDO1 (PDB: 4U74). (B) IC_{50} curve of IDO1 inhibition by TRYP. (C, D) Expression of IDO1 protein. All data were presented as the means ± SD (n = 3; *P <0.05 and **P <0.01).

After that, we simulated the molecular dynamic system of TRYP to IDO1. As shown in Figure 8A, the RMSD value was 0.21 at the end of the simulation, and the RMSD system was relatively stable after 10 ns. As shown in Figure 8B, except for residues at both ends, the fluctuations of residues at other positions were small, indicating that it was a flexible region in the molecule. Figure 6C shows little change in R_g values throughout the simulation and indicates little change in protein shape. Figure 6D shows how the number of secondary structures of protein changed over time. Figure 6E shows that the solvent-accessible surface area of proteins tended to decrease during the whole simulation phase.

3.7. *In Silico* ADMET Prediction about TRYP. At the first stage of the drug discovery process, *in silico* ADMET (absorption, distribution, metabolism, excretion, and toxicity) prediction is a crucial analysis to roll out undesirable effects of a proposed drug candidate.[50−52] In this regard, we used the Web tool SwissADME (http://www.swissadme.ch) to perform *in silico* ADMET analysis for TRYP in Table 2.

On the other hand, the BOILED-Egg plot between WLOGP and TPSA was used to predict gastrointestinal absorption and brain penetration. As shown in Figure 9, TRYP showed satisfactory gastrointestinal (GI) absorption and blood−brain barrier (BBB) permeability.

3.8. Effect of TRYP on Tumor Growth in Mice. A nude mouse model of CRC transplantation was established to verify whether TRYP inhibited tumor proliferation *in vivo*.[53] As shown in Figure 10A,B, the inhibitory effect of high and medium doses of TRYP on the volume of tumor growth was significant. However, the effects on the body weight of the mice were small, and no mouse death occurred during the experiment. As shown in Figure 10C,D, the tumor volume in the TRYP administration group decreased significantly. In depth, with an increase in the dose of TRYP, the tumor weight of the transplanted mice gradually decreased.

3.9. TRYP Improved Histopathological Changes in Mice. The effects of TRYP on hearts, livers, spleens, lungs, and kidneys were also tested. As shown in Figure 11A, different doses of TRYP (50, 100, and 200 mg/kg) did not significantly change the organ index of the mice with transplanted tumors. By contrast, tumor tissues were inhibited to various degrees (Figure 11B). This indicated that TRYP had a favorable anticancer effect *in vivo*.

3.10. Effect of TRYP on Ki67 and Apoptotic Signals from Tumor Tissue. Ki67 is a part of oncogenesis and can be used to predict the prognosis in colon adenocarcinoma.[54,55] IHC examination revealed that the expression levels of Ki67 were downregulated in tumor tissues from various doses of TRYP (50, 100, and 200 mg/kg) or the positive drug *in vivo*. As shown in Figure 12A,B, the proportion of Ki67 was significantly decreased (22.35 ± 0.01, 20.04 ± 0.01, and 17.26 ± 0.03%) compared with the model group (27.78 ± 0.03%). A TUNEL assay was used to detect the expression of apoptotic signals in tumor tissues. As shown in Figure 12C,D, the intensity of the apoptosis signal was effectively increased (80.54 ± 1.63, 112.69 ± 10.33, and 129.31 ± 1.95%) compared with the model group (70.43 ± 4.31%). The results showed that TRYP promoted the apoptosis of tumor cells *in vivo*. The above results indicated that TRYP inhibited tumor growth *in vivo* and exhibited excellent antitumor activity.

4. DISCUSSION

For the excellent anti-inflammatory effects of TRYP on dextran sulfate sodium-induced colitis and the important role of inflammation in the progression of cancer,[56,57] TRYP was used to test the antitumor effects on CRC. This study investigated

https://doi.org/10.1021/acsomega.4c11189
ACS Omega 2025, 10, 3206−3221

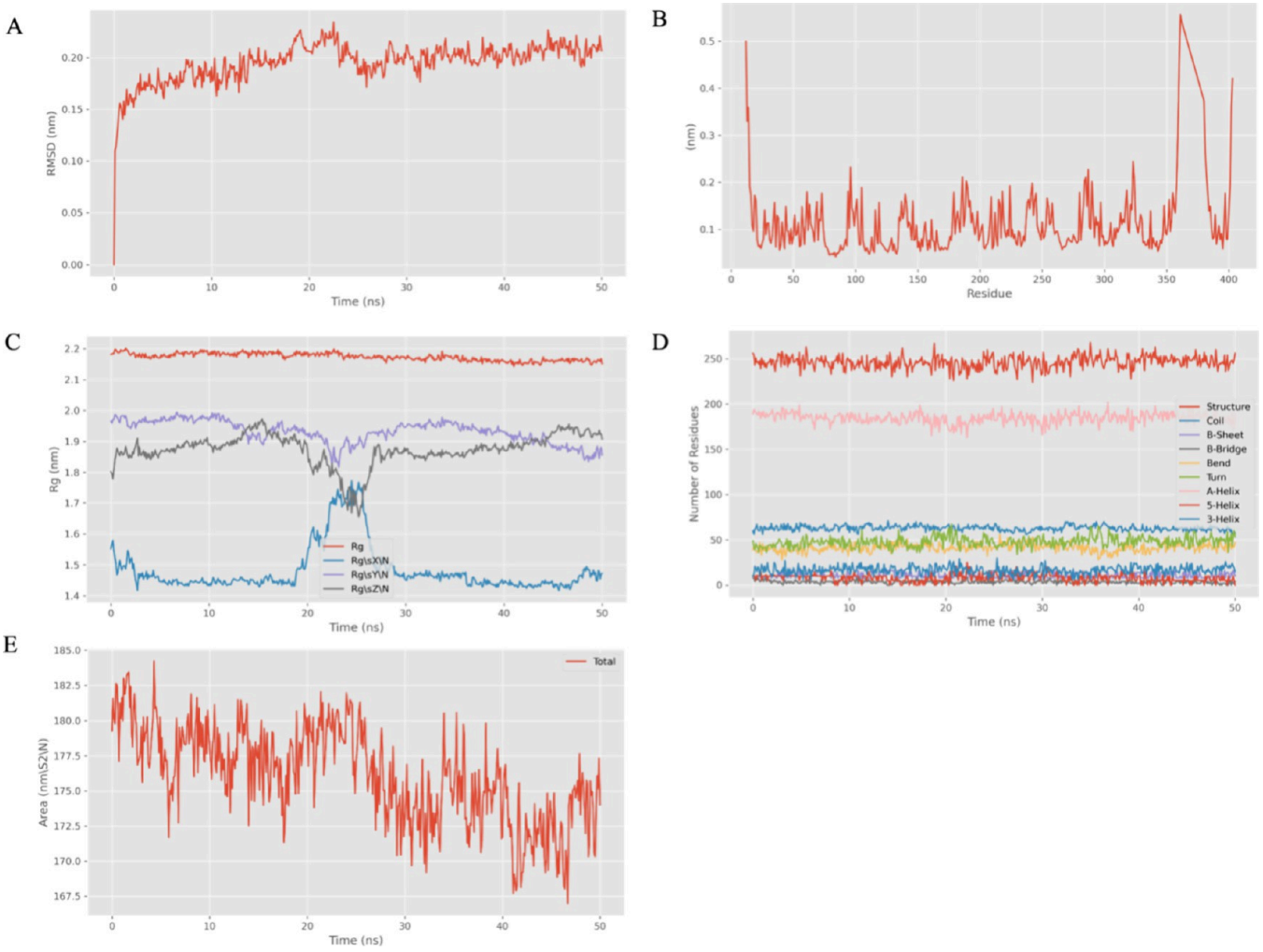

Figure 8. Molecular dynamics of IDO1. (A) RMSD curve of small protein molecules over time. (B) RMSF curves of different protein residues. (C) R_g curve of proteins over time. (D) Number of secondary structures in a protein changes over time. (E) Variation of the solvent-accessible surface area of the protein over time.

Table 2. *In Silico* ADMET Prediction about TRYP

physicochemical property	formal	$C_{15}H_8N_2O_2$
	MW[a]	248.24 g/mol
	TPSA[b]	51.96 Å
lipophilicity	log $P_{O/W}$[c]	2.16
water solubility	log S[d]	−3.29
pharmacokinetics	BBB[e]	yes
	log K_p[f]	−6.36 cm/s
drug-likeness[g]	Lipinski	yes
	Ghose	yes
	Veber	yes
	Egan	yes
	Muegge	yes
medicinal chemistry	SA[h]	2.42

[a]Molecular weight (MW). [b]Topological polar surface area (TPSA). [c]Partition coefficient between *n*-octanol and water (log $P_{O/W}$). [d]Logarithm of the solubility of a compound in a saturated aqueous solution (log S). [e]Blood−brain barrier (BBB) permeation. [f]Skin permeability coefficient (log K_p). [g]Assess qualitatively the chance for a molecule to become an oral drug with respect to bioavailability. [h]Synthetic accessibility (SA).

the inhibitory effects of TRYP on the growth of SW620 cells and analyzed the underlying mechanisms. *In vitro*, the outcomes confirmed that TRYP dramatically inhibited the proliferation of SW620 cells in a time- and concentration-dependent manner. Moreover, TRYP treatment arrested the cell cycle at the S phase. However, SW620 cells had characteristics of aggregation growth and were difficult to migrate. In addition, TRYP could significantly induce the apoptosis of SW620 cells, and the Bcl-2 expression level was alleviated, while expression levels of Bax and cleaved caspase 3 were enhanced, which played an important role in antitumor activity. These findings demonstrated that TRYP could regulate proliferation and migration of SW620 cells, arrest the cell cycle at the S phase, and induce the apoptosis of SW620 cells.

According to transcriptome database analysis, the effect of TRYP on SW620 cells was tightly connected with the MAPK signaling pathway. Therefore, the main proteins involved in the MAPK signaling pathway were identified. The result showed that decreasing the expression levels of p-Erk and increasing the expression levels of p-P38 and p-Jnk activate the MAPK signaling pathway, inhibiting the proliferation of SW620 cells and inducing apoptosis. These results indicated that the inhibitory effects of TRYP on SW620 cells were closely related to the regulation of the expression of the MAPK signaling pathway.

https://doi.org/10.1021/acsomega.4c11189
ACS Omega 2025, 10, 3206−3221

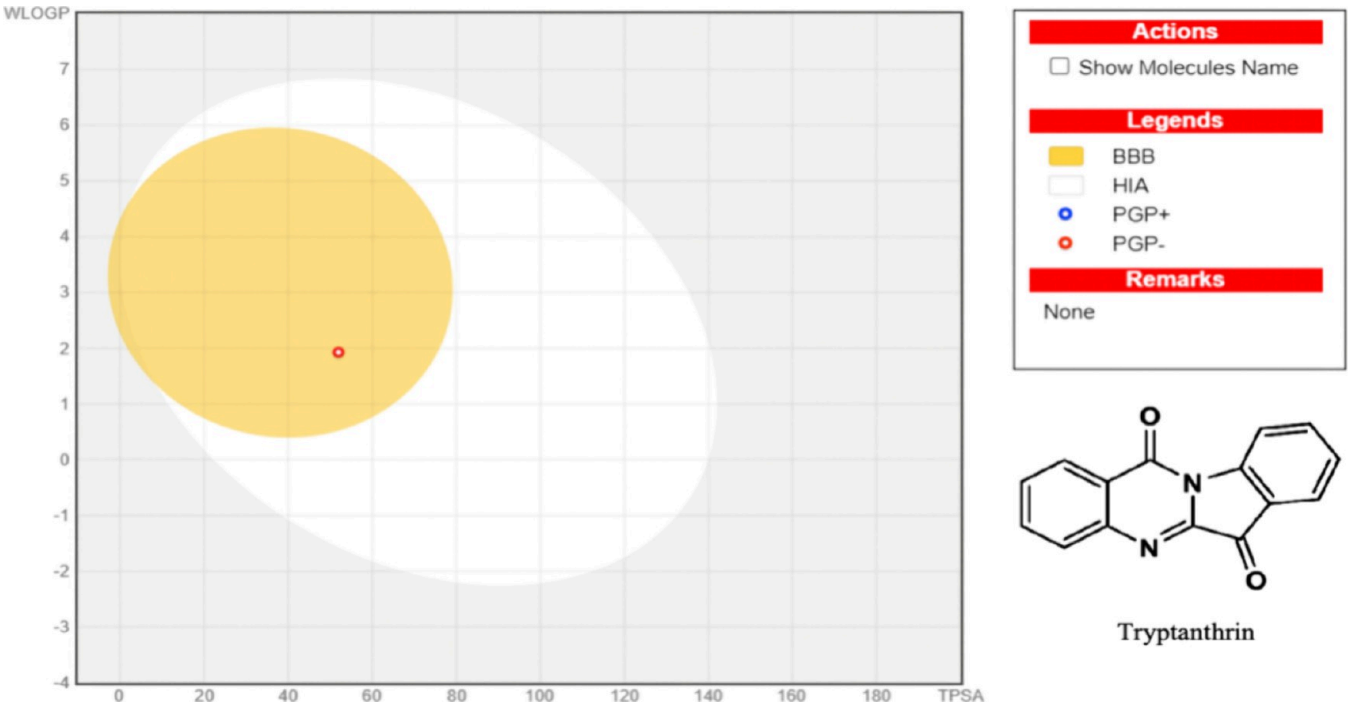

Figure 9. BOILED-Egg plot of TRYP.

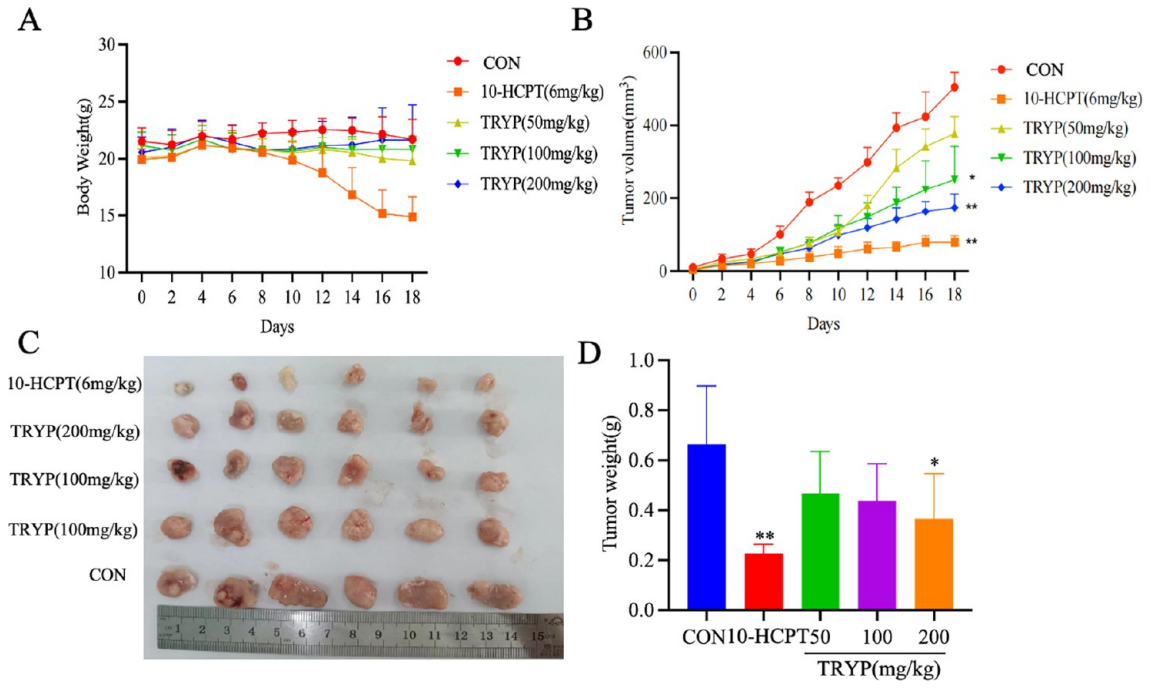

Figure 10. Effect of TRYP on tumor growth in mice. (A) Effects of TRYP on body weight. (B) Effects of TRYP on the tumor volume of mice. (C, D) Tumor volume and weight in mice. All data were presented as the means ± SD (n = 3; *P < 0.05 and **P < 0.01).

Because previous studies had shown that the activity of Topo I at the S phase was significantly increased, it was predicted that TRYP might inhibit the activity of Topo I. Therefore, the activity of Topo I was detected *in virto*, and the molecule docking was used to calculate the binding sites of TRYP and Topo I. Fortunately, the experiments verified our hypothesis. And it was the first to discover TRYP could inhibit Topo I. IDO1 was exerted important roles in tryptophan metabolism. And it was also reported that TRYP and its derivatives could inhibit IDO1. Our results once again demonstrated TRYP could inhibit the activation of IDO1 on SW620 cells. Moreover, both Topo I and IDO1 maintained a strong and stable interaction with TRYP during MD simulations. At the same time, we performed ADMET prediction, and the results showed that TRYP possessed satisfactory lipophilicity, water solubility, GI absorption and BBB permeability. And it could successfully be passed fundamental drug-likeness filters, including Lipinski (Pfizer), Ghose (Amgen), Veber (GSK), Egan (Pharmacia), and Muegge (Bayer).

https://doi.org/10.1021/acsomega.4c11189
ACS Omega 2025, 10, 3206−3221

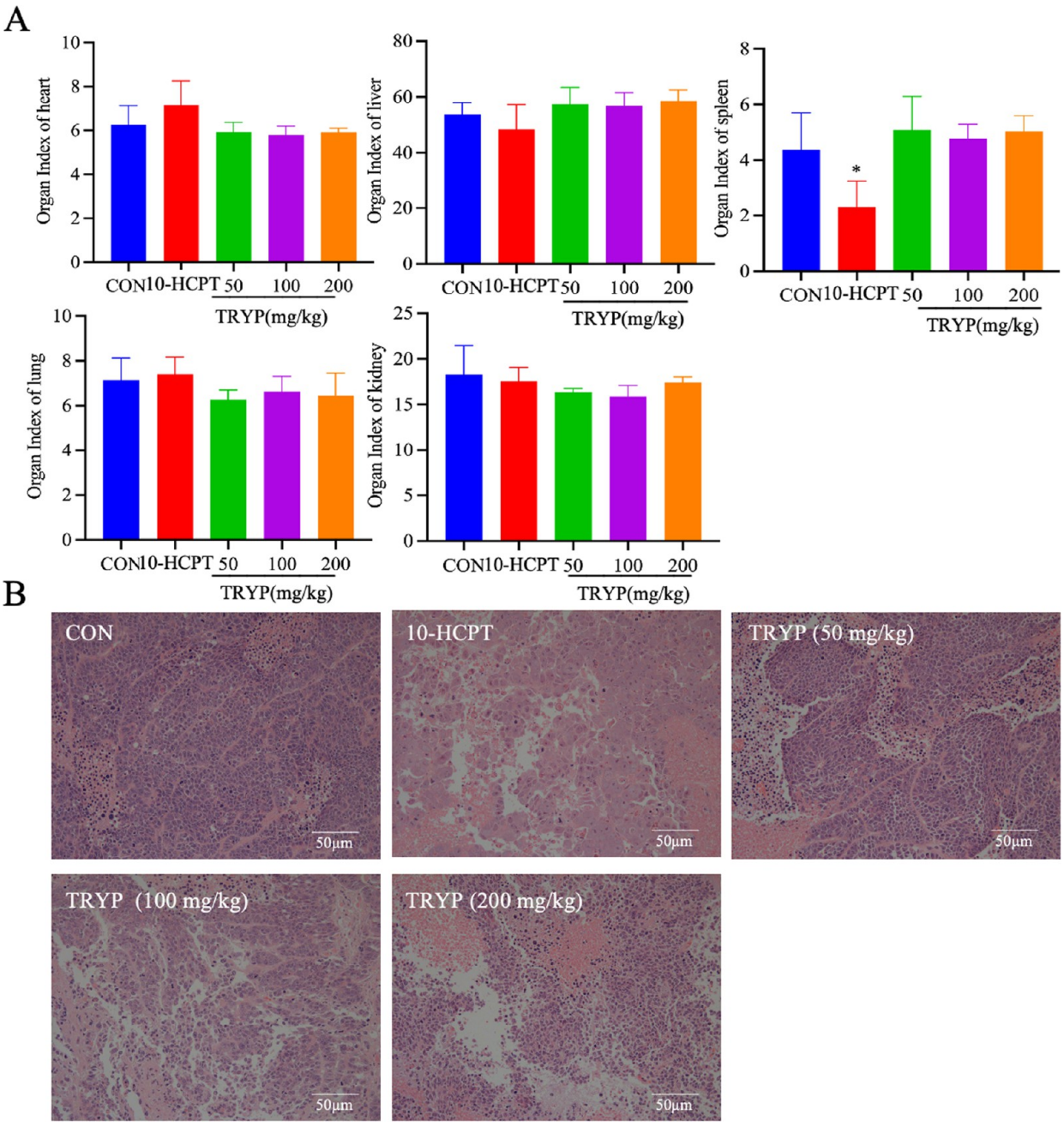

Figure 11. TRYP improved histopathological changes in mice. (A) Effect of TRYP on the organ index of mice. All data were presented as the means ± SD (n = 3; *P < 0.05 and **P < 0.01). (B) H&E staining of tumor tissues. Images were acquired at 20×. Scale bars, 50 μm.

The antitumor effects of TRYP were evaluated *in vivo* using models of transplantable subcutaneous tumors in mice. The results demonstrated that TRYP inhibited tumor growth in mice but had no significant effect on body weight or spleen index. In addition, TRYP significantly promoted SW620 cell apoptosis and inhibited tumor growth. Meanwhile, the positive expression of Ki67 in the tumor tissues of transplanted mice decreased to different degrees. In contrast, the apoptotic fluorescence intensity increased to different degrees. These results suggested that TRYP inhibited tumor growth *in vivo*.

MAPK, Topo I, and IDO1 were important targets and signaling pathway, where they were inhibited by a variety of compounds to effectively treat tumors.[58−60] TRYP targeted to Topo I and IDO1 modulated the MAPK signaling pathway, which provided a multitargeted therapeutic way for cancer. Thus, TRYP might play a better antitumor role. Further, TRYP had the advantages of availability and fewer side effects. Hence, TRYP could be used in combination with other known therapies in the future, in particular with Topo I, IDO1, and the MAPK signaling pathway.

5. CONCLUSIONS

In summary, our findings indicated that TRYP not only inhibits the proliferation of SW620 cells but also induces apoptosis. The underlying mechanism might be related to regulation of the MAPK signaling pathway and inhibition of Topo I and IDO1. TRYP effectively inhibited the growth of transplanted tumors in nude mice and exhibited good antitumor activity. Therefore, TRYP is a potential target for CRC treatment. This study provides a comprehensive

https://doi.org/10.1021/acsomega.4c11189
ACS Omega 2025, 10, 3206−3221

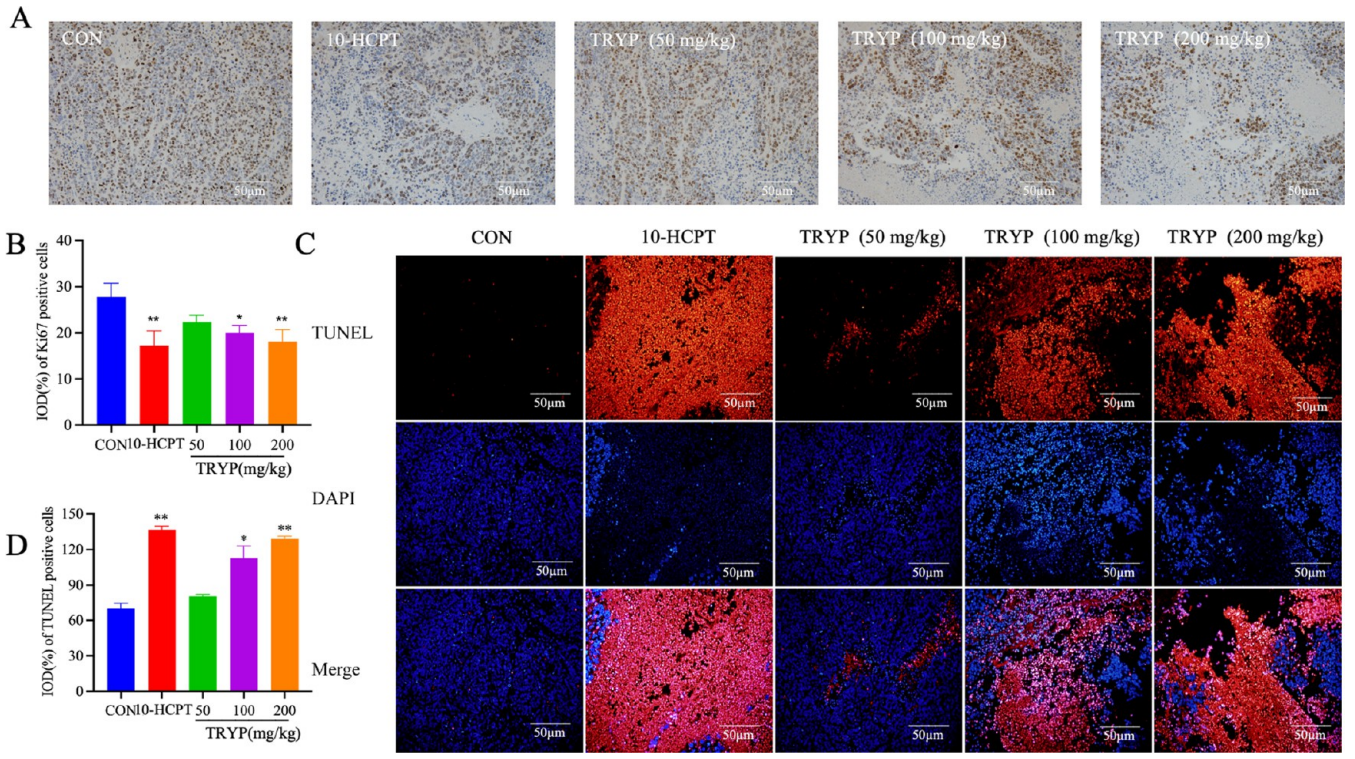

Figure 12. Effect of TRYP on Ki67 and apoptotic signals from tumor tissue. (A, B) IHC analyses of Ki67 expression in tumor tissues. All data were presented as the means ± SD (n = 3; *P < 0.05 and **P < 0.01). Images were acquired at 20×. Scale bars, 50 μm. (C, D) Results of TUNEL immunofluorescence in tumor tissues. All data were presented as the means ± SD (n = 3; *P < 0.05 and **P < 0.01). Images were acquired at 20×. Scale bar, 50 μm.

understanding of the potential molecular mechanism by which TRYP exerts its effects, paving the way for its consideration as a novel treatment option in CRC management.

AUTHOR INFORMATION

Corresponding Authors

Xue Wu − *Medical Experiment Center, Shaanxi University of Chinese Medicine, Xianyang, Shaanxi 712046, China*; Email: wuxue0820@163.com

Yan-Ni Liang − *Co-construction Collaborative Innovation Center of Chinese Medicine Resources Industrialization by Shaanxi & Education Ministry, State Key Laboratory of Research & Development of Characteristic Qin Medicine Resources (Cultivation), Shaanxi University of Chinese Medicine, Xianyang, Shaanxi 712046, China*; Email: aiziji_2005@126.com

Zheng Wang − *Co-construction Collaborative Innovation Center of Chinese Medicine Resources Industrialization by Shaanxi & Education Ministry, State Key Laboratory of Research & Development of Characteristic Qin Medicine Resources (Cultivation), Shaanxi University of Chinese Medicine, Xianyang, Shaanxi 712046, China*; Email: wazh0405@126.com

Authors

Simeng Lu − *Co-construction Collaborative Innovation Center of Chinese Medicine Resources Industrialization by Shaanxi & Education Ministry, State Key Laboratory of Research & Development of Characteristic Qin Medicine Resources (Cultivation), Shaanxi University of Chinese Medicine, Xianyang, Shaanxi 712046, China*; orcid.org/0009-0006-7428-1986

Bao-Long Hou − *Co-construction Collaborative Innovation Center of Chinese Medicine Resources Industrialization by Shaanxi & Education Ministry, State Key Laboratory of Research & Development of Characteristic Qin Medicine Resources (Cultivation), Shaanxi University of Chinese Medicine, Xianyang, Shaanxi 712046, China*

Ting Wang − *Co-construction Collaborative Innovation Center of Chinese Medicine Resources Industrialization by Shaanxi & Education Ministry, State Key Laboratory of Research & Development of Characteristic Qin Medicine Resources (Cultivation), Shaanxi University of Chinese Medicine, Xianyang, Shaanxi 712046, China*

Keyu Ma − *Co-construction Collaborative Innovation Center of Chinese Medicine Resources Industrialization by Shaanxi & Education Ministry, State Key Laboratory of Research & Development of Characteristic Qin Medicine Resources (Cultivation), Shaanxi University of Chinese Medicine, Xianyang, Shaanxi 712046, China*

Anli Huang − *Co-construction Collaborative Innovation Center of Chinese Medicine Resources Industrialization by Shaanxi & Education Ministry, State Key Laboratory of Research & Development of Characteristic Qin Medicine Resources (Cultivation), Shaanxi University of Chinese Medicine, Xianyang, Shaanxi 712046, China*

Complete contact information is available at: https://pubs.acs.org/10.1021/acsomega.4c11189

Author Contributions

[1]S.L., B.-L.H., and T.W. contributed equally to this work.

https://doi.org/10.1021/acsomega.4c11189
ACS Omega 2025, 10, 3206−3221

Author Contributions

Simeng Lu: methodology, validation, formal analysis, investigation, and writing of the original draft. Bao-Long Hou: review and editing, validation, formal analysis, and investigation. Ting Wang: methodology, validation, formal analysis, and investigation. Keyu Ma: visualization. Anli Huang: visualization. Xue Wu: methodology. Yan-Ni Liang: review, editing, and funding acquisition. Zheng Wang: review, editing, and funding acquisition.

Funding

This study was supported by the Key Research and Development Program of Shaanxi Province (2018ZDCXL-SF-01-02-02 and 2022SF-139).

Notes

The authors declare no competing financial interest.

All animal experiments were conducted according to the scheme approved by the animal ethics committee of Shaanxi University of Chinese Medicine. The approval code is SUCMDL2022120100.

■ ACKNOWLEDGMENTS

We would like to thank the Youth Innovation Team of Shaanxi Universities (Education Department of Shaanxi Provincial Government [2019], no. 90).

■ REFERENCES

(1) Akimoto, N.; Ugai, T.; Zhong, R.; Hamada, T.; Fujiyoshi, K.; Giannakis, M.; Wu, K.; Cao, Y.; Ng, K.; Ogino, S. Rising incidence of early-onset colorectal cancer - a call to action. *Nat. Rev. Clin. Oncol.* **2021**, *18* (4), 230−243.

(2) Wijnands, A. M.; Jong, M. E. D.; Lutgens, M. W. M. D.; Hoentjen, F.; Elias, S. G. E.; Oldenburg, B. Prognostic Factors for Advanced Colorectal Neoplasia in Inflammatory Bowel Disease: Systematic Review and Meta-analysis. *Gastroenterology* **2021**, *160* (5), 1584−1598.

(3) Rutter, M.; Saunders, B.; Wilkinson, K.; Rumbles, S.; Schofield, G.; Kamm, M.; Williams, C.; Price, A.; Talbot, I.; Forbes, Ar Severity of inflammation is a risk factor for colorectal neoplasia in ulcerative colitis. *Gastroenterology* **2004**, *126* (2), 451−459.

(4) Liang, Q.; Ma, D.; Zhu, X.; Wang, Z.; Sun, T. T.; Shen, C.; Yan, T.; Tian, X.; Yu, T.; Guo, F.; Tang, J.; Lin, Y.; Chen, H.; Zhou, C.; Ge, Z.; Zhong, M.; Chen, J.; Liu, Q.; Wang, Z.; Fang, J. Y.; Chen, H.; Hong, J. RING-Finger Protein 6 Amplification Activates JAK/STAT3 Pathway by Modifying SHP-1 Ubiquitylation and Associates with Poor Outcome in Colorectal Cancer. *Clin. Cancer. Res.* **2018**, *24* (6), 1473−1485.

(5) Wang, Z.; Chang, Y.; Sun, H.; Li, Y.; Tang, T. Advances in molecular mechanisms of inflammatory bowel disease-associated colorectal cancer (Review). *Oncol. Lett.* **2024**, *27* (6), 257.

(6) Hossein, M. A comprehensive survey upon diverse and prolific applications of chitosan-based catalytic systems in one-pot multi-component synthesis of heterocyclic rings. *Int. J. Biol. Macromol.* **2021**, *186*, 1003−1166.

(7) Pal, R.; Matada, S. P. M.; Teli, G.; Saha, M.; Patel, R. Therapeutic potential of anticancer activity of nitrogen-containing heterocyclic scaffolds as Janus kinase (JAK) inhibitor: Biological activity, selectivity, and structure−activity relationship. *Bioorg. Chem.* **2024**, *152*, No. 107696.

(8) Hossein, M. A concise and focused overview upon arylglyoxal monohydrates-based one-pot multi-component synthesis of fascinating potentially biologically active pyridazines. *J. Mol. Struct.* **2022**, *1251*, No. 131742.

(9) Marshall, C. M.; Federice, J. G.; Bell, C. N.; Cox, P. B.; Njardarson, J. T. An Update on the Nitrogen Heterocycle Compositions and Properties of U.S. FDA-Approved Pharmaceuticals (2013−2023). *J. Med. Chem.* **2024**, *67* (14), 11622−11655.

(10) Luo, W.; Liu, Y.; Qin, H.; Zhao, Z.; Wang, S.; He, W.; Tang, S.; Peng, Mei Nitrogen-containing heterocyclic drug products approved by the FDA in 2023: Synthesis and biological activity. *Eur. J. Med. Chem.* **2024**, *279*, No. 116838.

(11) Zhou, X. Recent advances of tryptanthrin and its derivatives as potential anticancer agents. *RSC. Med. Chem.* **2024**, *15* (4), 1127−1147.

(12) Kaur, R.; Manjal, S. K.; Rawal, R. K.; Kumar, Kapil Recent synthetic and medicinal perspectives of tryptanthrin. *Bioorg. Med. Chem.* **2017**, *25* (17), 4533−4552.

(13) Honda, G.; Tosirisuk, V.; Tabata, M. Isolation of an antidermatophytic, tryptanthrin, from indigo plants, Polygonum tinctorium and Isatis tinctoria. *Planta. Med.* **1980**, *38* (3), 275−276.

(14) Tsai, Y. C.; Lee, C. L.; Yen, H. R.; Chang, Y. S.; Lin, Y. P.; Huang, S. H.; Lin, C. W. Antiviral Action of Tryptanthrin Isolated from Strobilanthes cusia Leaf against Human Coronavirus NL63. *Biomolecules* **2020**, *10* (3), 366.

(15) Chang, H. N.; Huang, S. T.; Yeh, Y. C.; Wang, H. S.; Wang, T. H.; Wu, Y. H.; Pang, J. H. Indigo naturalis and its component tryptanthrin exert anti-angiogenic effect by arresting cell cycle and inhibiting Akt and FAK signaling in human vascular endothelial cells. *J. Ethnopharmacol.* **2015**, *174*, 474−481.

(16) Zeng, Q.; Luo, C.; Cho, J.; Lai, D.; Shen, X.; Zhang, X.; Zhou, W. Tryptanthrin exerts anti-breast cancer effects both in vitro and in vivo through modulating the inflammatory tumor microenvironment. *Acta. Pharm.* **2021**, *71* (2), 245−266.

(17) Ishihara, T.; Kohno, K.; Ushio, S.; Iwaki, K.; Ikeda, M.; Kurimoto, M. Tryptanthrin inhibits nitric oxide and prostaglandin E(2) synthesis by murine macrophages. *Eur. J. Pharmacol.* **2000**, *407* (1−2), 197−204.

(18) Wang, Z.; Wu, X.; Wang, C. L.; Wang, L.; Sun, C.; Zhang, D. B.; Liu, J. L.; Liang, Y. N.; Tang, D. X.; Tang, Z. S. Tryptanthrin Protects Mice against Dextran Sulfate Sodium-Induced Colitis through Inhibition of TNF-α/NF-κB and IL-6/STAT3 Pathways. *Molecules* **2018**, *23* (5), 1062.

(19) Wagner, E. F.; Nebreda, A. R. Signal integration by JNK and p38 MAPK pathways in cancer development. *Nat. Rev. Cancer.* **2009**, *9* (8), 537−549.

(20) Sun, Y.; Liu, W. Z.; Liu, T.; Feng, X.; Yang, N.; Zhou, H. F. Signaling pathway of MAPK/ERK in cell proliferation, differentiation, migration, senescence and apoptosis. *J. Recept. Signal. Transduct. Res.* **2015**, *35* (6), 600−604.

(21) Samatar, A. A.; Poulikakos, P. I. Targeting RAS-ERK signalling in cancer: promises and challenges. *Nat. Rev. Drug. Discovery* **2014**, *13* (12), 928−942.

(22) Fang, J. Y.; Richardson, B. C. The MAPK signalling pathways and colorectal cancer. *Lancet. Oncol.* **2005**, *6* (5), 322−327.

(23) Xiong, Y.; Wang, J.; Wang, S.; Li, H.; Zhou, X. Trydptanthrin ameliorates imiquimod-induced psoriasis in mice by suppressing inflammation and oxidative stress via NF-κB/MAPK/Nrf2 pathways. *J. Nat. Med.* **2023**, *77* (1), 188−201.

(24) Champoux, J. J. DNA topoisomerases: structure, function, and mechanism. *Annu. Rev. Biochem.* **2001**, *70*, 369−413.

(25) Qi, J.; Zheng, Y.; Li, B.; Ai, Y.; Chen, M.; Zheng, X. Pyridoxal hydrochloride thiosemicarbazones with copper ions inhibit cell division via Topo-I and Topo-IIα. *J. Inorg. Biochem.* **2022**, *232*, No. 111816.

(26) Singh, A.; Kaur, N.; Singh, G.; Sharma, P.; Bedi, P.; Sharma, S.; Nepali, K. Topoisomerase I and II Inhibitors: A Patent Review. *Recent. Pat. Anticancer. Drug. Discovery* **2016**, *11* (4), 401−423.

(27) Liu, Y. P.; Chen, H. L.; Tzeng, C. C.; Lu, P. J.; Lo, C. W.; Lee, Y. C.; Tseng, C. H.; Chen, Y. L.; Yang, C. N. TCH-1030 targeting on topoisomerase I induces S-phase arrest, DNA fragmentation, and cell death of breast cancer cells. *Breast. Cancer. Res. Treat.* **2013**, *138* (2), 383−393.

(28) Li, T.; Zhou, A. D.; Bai, L. F.; Zhang, X. Y.; Zhou, Y. T.; Yang, H. L.; Xu, L. T.; Guo, X. Q.; Zhu, X. Y.; Wang, D. J.; Gu, H. W.; Wang, X. M. Design, synthesis, and anticancer activity of three novel palbociclib derivatives. *Front. Oncol.* **2022**, *12*, No. 959322.

https://doi.org/10.1021/acsomega.4c11189
ACS Omega 2025, 10, 3206−3221

(29) Röhrig, U. F.; Michielin, O.; Zoete, V. Structure and Plasticity of Indoleamine 2,3-Dioxygenase 1 (IDO1). *J. Med. Chem.* **2021**, *64* (24), 17690−17705.
(30) Ariel, L. B.; Khoa, N. P.; Batabyal, D.; Karkashon, S.; Bonanno, J. B.; Poulos, T. L.; Yeh, S. Ru Structural insights into substrate and inhibitor binding sites in human indoleamine 2,3-dioxygenase 1. *Nat. Commun.* **2017**, *8* (1), 1693.
(31) Hossein, M.; Rimaz, M.; Zeynizadeh, B. Practical Three-Component Regioselective Synthesis of Drug-Like 3-Aryl(or hetero-aryl)-5,6-dihydrobenzo[h]cinnolines as Potential Non-Covalent Multi-Targeting Inhibitors To Combat Neurodegenerative Diseases. *ACS. Chem. Neurosci.* **2024**, *15* (9), 1828−1881.
(32) Yang, D.; Zhang, S.; Fang, X.; Guo, L.; Hu, N.; Guo, Z.; Li, X.; Yang, S.; He, J. C.; Kuang, C.; Yang, Q. N-Benzyl/Aryl Substituted Tryptanthrin as Dual Inhibitors of Indoleamine 2,3-Dioxygenase and Tryptophan 2,3-Dioxygenase. *J. Med. Chem.* **2019**, *62* (20), 9161−9174.
(33) Li, Y.; Zhang, S.; Wang, R.; Cui, M.; Liu, W.; Yang, Q.; Kuang, C. Synthesis of novel tryptanthrin derivatives as dual inhibitors of indoleamine 2,3-dioxygenase 1 and tryptophan 2,3-dioxygenase. *Bioorg. Med. Chem. Lett.* **2020**, *30* (11), No. 127159.
(34) Afsan, Z.; Roisnel, T.; Tabassum, S.; Arjmand, F. Structure elucidation (Afsan, Roisnel et al. 2020) of new tailored benzene-sulfonamide derived Schiff base copper(II) intercalating complexes: Comprehensive biological profile {DNA binding, pBR322 DNA cleavage, Topo I inhibition and cytotoxic activity}. *Bioorg. Chem.* **2020**, *94*, No. 103427.
(35) Sadok, I.; Rachwał, K.; Jonik, I.; Staniszewska, M. Reliable chromatographic assay for measuring of indoleamine 2,3-dioxygenase 1 (IDO1) activity in human cancer cells. *J. Enzyme. Inhib. Med. Chem.* **2021**, *36* (1), 581−592.
(36) Tu, J.; Li, J. J.; Song, L. T.; Zhai, H. L.; Wang, J.; Zhang, X. Y. Molecular modeling study on resistance of WT/D473H SMO to antagonists LDE-225 and LEQ-506. *Pharmacol. Res.* **2018**, *129*, 491−499.
(37) Mohammad, R. M.; Muqbil, I.; Lowe, L.; Yedjou, C.; Hsu, H. Y.; Lin, L. T.; Siegelin, M. D.; Fimognari, C.; Kumar, N. B.; Dou, Q. P.; Yang, H.; Samadi, A.; Russo, G. L.; Spagnuolo, C.; Ray, S. K.; Chakrabarti, M.; Morre, J. D.; Coley, H. M.; Honoki, K.; Fujii, H.; Georgakilas, A. G.; Amedei, A.; Nicoolai, E.; Amin, A.; Ashraf, S. S.; Helferich, W. G.; Yang, X.; Boosani, C. S.; Guha, G.; Bhakta, D.; Ciriolo, M. R.; Aquilano, K.; Chen, S.; Mohammed, S. I.; Keith, W. N.; Bilsland, A.; Halicka, D.; Nowsheen, S.; Azmi, A. S. Broad targeting of resistance to apoptosis in cancer. *Semin. Cancer. Biol.* **2015**, *35 suppl* (0), S78−S103.
(38) Chang, I.; Majid, S.; Saini, S.; Zaman, M. S.; Yamamura, S.; Chiyomaru, T.; Shahryari, V.; Fukuhara, S.; Deng, G.; Dahiya, R.; Tanaka, Y. Hrk mediates 2-methoxyestradiol-induced mitochondrial apoptotic signaling in prostate cancer cells. *Mol. Cancer. Ther.* **2013**, *12* (6), 1049−1059.
(39) Atthapaan, M.; Yasamut, U.; Netsawang, J.; Noisakran, S.; Wongwiwat, W.; Songprakhon, P.; Srisawat, C.; Puttikhunt, C.; Kasinrerk, W.; Malasit, P.; Yenchitsomanus, P. T.; Limjindaporn, T. Cell death gene expression profile: role of RIPK2 in dengue virus-mediated apoptosis. *Virus. Res.* **2011**, *156* (1−2), 25−34.
(40) He, L.; Li, H.; Pan, C.; Hua, Y.; Peng, J.; Zhou, Z.; Zhao, Y.; Lin, M. Squalene epoxidase promotes colorectal cancer cell proliferation through accumulating calcitriol and activating CYP24A1-mediated MAPK signaling. Cancer Commun. *Cancer Commun. (lond)* **2021**, *41* (8), 726−746.
(41) Dong, F.; Tian, H.; Yan, S.; Li, L.; Dong, X.; Wang, F.; Li, J.; Li, C.; Cao, Z.; Liu, X.; Liu, J. Dihydroartemisinin inhibits endothelial cell proliferation through the suppression of the ERK signaling pathway. *Int. J. Mol. Med.* **2015**, *35* (3), 1381−1387.
(42) You, L.; Ren, X.; Du, Y.; Zhao, W.; Cui, M.; Chen, G.; Zhao, Y. c-Fos/ERK promotes the progression from pancreatic intraepithelial neoplasia to pancreatic ductal adenocarcinoma. *Oncol. Rep.* **2016**, *36* (6), 3413−3420.
(43) Znojek, P.; Willmore, E.; Curtin, N. J. Preferential potentiation of topoisomerase I poison cytotoxicity by PARP inhibition in S phase. *Br. J. Cancer.* **2014**, *111* (7), 1319−1326.
(44) Sabe, V. T.; Ntombela, T.; Jhamba, L. A.; Maguire, G. E. M.; Govender, T.; Naicker, T.; Kruger, H. G. Current trends in computer aided drug design and a highlight of drugs discovered via computational techniques: A review. *Eur. J. Med. Chem.* **2021**, *224*, No. 113705.
(45) Siddiquee, N. H.; Hossain, M. I.; Talukder, M. E. K.; Nirob, S. A. A.; Shourav, M.; Jahan, I.; Tamanna, U. H. A.; Das, P.; Akter, R.; Hasan, M.; Mamun, M. A. A.; Saha, O. In-silico identification of novel natural drug leads against the Ebola virus VP40 protein: A promising approach for developing new antiviral therapeutics. *Inform. Med. Unlocked* **2024**, *45*, No. 101458.
(46) Cox, P. B.; Gupta, R. Contemporary Computational Applications and Tools in Drug Discovery. *ACS. Med. Chem. Lett.* **2022**, *13* (7), 1016−1029.
(47) Mousavi, H.; Zeynizadeh, B.; Rimaz, M. Green and efficient one-pot three-component synthesis of novel drug-like furo[2,3-d]pyrimidines as potential active site inhibitors and putative allosteric hotspots modulators of both SARS-CoV-2 M^{Pro} and PL^{Pro}. *Bioorg. Chem.* **2023**, *135*, No. 106390.
(48) Yang, S.; Li, X.; Hu, F.; Li, Y.; Yang, Y.; Yan, J.; Kuang, C.; Yang, Q. Discovery of tryptanthrin derivatives as potent inhibitors of indoleamine 2,3-dioxygenase with therapeutic activity in Lewis lung cancer (LLC) tumor-bearing mice. *J. Med. Chem.* **2013**, *56* (21), 8321−8331.
(49) Yang, Y.; Jin, Y.; Yin, L.; Liu, P.; Zhu, L.; Gao, H. Sertaconazole nitrate targets IDO1 and regulates the MAPK signaling pathway to induce autophagy and apoptosis in CRC cells. *Eur. J. Pharmacol.* **2023**, *942*, No. 175515.
(50) Jia, C. Y.; Li, J. Y.; Hao, G. F.; Yang, G. F. A drug-likeness toolbox facilitates ADMET study in drug discovery. *Drug. Discovery Today.* **2020**, *25* (1), 248−258.
(51) Feinberg, E. V.; Joshi, E.; Pande, V. S.; Cheng, A. C. Improvement in ADMET prediction with multitask deep featurization. *J. Med. Chem.* **2020**, *63* (16), 8835−8848.
(52) Ferreira, L. L. G.; Andricopulo, A. D. ADMET modeling approaches in drug discovery. *Drug. Discovery Today.* **2019**, *24* (5), 1157−1165.
(53) Zhao, T.; Li, Y.; Shen, K.; Wang, Q.; Zhang, J. Knockdown of OLR1 weakens glycolytic metabolism to repress colon cancer cell proliferation and chemoresistance by downregulating SULT2B1 via c-MYC. *Cell. Death. Dis.* **2021**, *13* (1), 4.
(54) Ayerden, D.; Tayfur, M.; Balci, M. G. Comparison of histopathological findings of the colon adenomas and adenocarcinomas with cyclin D1 and Ki-67 expression. *Niger. J. Clin. Pract.* **2021**, *24* (11), 1737−1741.
(55) Ahmed Nor, E. M.; Saied, E. M.; Mina, S. N.; Shareef, M. M.; Abdelaziz, D. M. Clinicopathological Value Of Epidermal Growth Factor Receptor (EGFR) And Ki-67 Expression In Colorectal Adenoma And Adenocarcinoma. *J. Pak. Med. Assoc.* **2023**, *73* (Suppl 4) (4), S124−S130.
(56) Zhu, J.; Hou, B. L.; Cheng, W.; Wang, T.; Wang, Z.; Liang, Y. N. Mechanism of tryptanthrin in treatment of ulcerative colitis in mice based on serum metabolomics. *Zhongguo Zhong Yao Za Zhi* **2023**, *48* (8), 2193−2202.
(57) Singh, N.; Baby, D.; Rajguru, J. P.; Patil, P. B.; Thakkannavar, S. S.; Pujari, V. B. Inflammation and cancer. *Ann. Afr. Med.* **2019**, *18* (3), 121−126.
(58) Wang, C.; Yan, L.; Wang, Y.; Lin, B.; Liu, S.; Li, Q.; Gao, L.; Zhang, S.; Iwamori, M. Overexpression of Lewis(y) antigen protects ovarian cancer RMG-1 cells from carboplatin-induced apoptosis by the upregulation of Topo-I and Topo-II β. *Anat. Rec (Hoboken)* **2011**, *294* (6), 961−969.
(59) Zeitler, L.; Murray, P. J. L4i1 and IDO1: Oxidases that control a tryptophan metabolic nexus in cancer. *J. Biol. Chem.* **2023**, *299* (6), No. 104827.

https://doi.org/10.1021/acsomega.4c11189
ACS Omega 2025, 10, 3206−3221

(60) Bahar, M. E.; Kim, H. J.; Kim, D. R. Targeting the RAS/RAF/MAPK pathway for cancer therapy: from mechanism to clinical studies. *Signal. Transduct. Target. Ther.* **2023**, *8* (1), 455.

https://doi.org/10.1021/acsomega.4c11189
ACS Omega 2025, 10, 3206−3221